Composites Part B 81 (2015) 64–71

Contents lists available at ScienceDirect

Composites Part B

journal homepage: www.elsevier.com/locate/compositesb

A numerical study on carbon nanotube pullout to understand its bridging effect in carbon nanotube reinforced composites

Yuanyuan Jia [a], Zuorong Chen [b], Wenyi Yan [a, *]

[a] Department of Mechanical and Aerospace Engineering, Monash University, Wellington Road, Clayton, Victoria 3800, Australia
[b] CSIRO Earth Science & Resource Engineering, Clayton North, Victoria 3169, Australia

ARTICLE INFO

Article history:
Received 5 February 2015
Received in revised form
23 April 2015
Accepted 7 July 2015
Available online 15 July 2015

Keywords:
A. Carbon nanotube
B. Debonding
C. Finite element analysis (FEA)
Critical embedded length

ABSTRACT

Carbon nanotube (CNT) reinforced polymeric composites provide a promising future in structural engineering. To understand the bridging effect of CNT in the events of the fracture of CNT reinforced composites, the finite element method was applied to simulate a single CNT pullout from a polymeric matrix using cohesive zone modelling. The numerical results indicate that the debonding force during the CNT pullout increases almost linearly with the interfacial crack initiation shear stress. Specific pullout energy increases with the CNT embedded length, while it is independent of the CNT radius. In addition, a saturated debonding force exists corresponding to a critical CNT embedded length. A parametric study shows that a higher saturated debonding force can be achieved if the CNT has a larger radius or if the CNT/matrix has a stronger interfacial bonding. The critical CNT embedded length decreases with the increase of the interfacial crack initiation shear stress.

© 2015 Elsevier Ltd. All rights reserved.

1. Introduction

Nanocomposite is a multiphase solid material where one of the reinforcing materials is less than 100 nm [1]. Polymeric nanocomposite materials, which combine polymers with nano-additives, have attracted vast interest as a new material with many uses [2–4]. CNTs are the finest and strongest fibres with nanoscale diameter and length ranging from micro to millimetres [5]. They were discovered by Iijima in 1991 [6]. They are the ideal reinforcement for high performance composites due to their small size, low density, high stiffness and high strength; and therefore, considered as the new generation of reinforcing phase in fabricating nano-composite materials. Measurements used *in situ* transmission electron microscopy and atomic force microscopy show that the Young's modulus of CNTs is in the order of 1 TPa [7,8]. The tensile strength is up to 150 GPa [9]. CNTs are currently used in both conventional and novel areas, such as lightweight structural composites, field emission devices, and electronics. In the past few years, research has been carried out to better understand the mechanical performance of CNT reinforced composites. It showed that a small quantity of nanotubes added to a polymer matrix can increase the stiffness and strength of the composite [3,4]. For example, dispersing 1% wt of CNTs to a matrix material results in up to 42% increase in the stiffness of the composite [3]. However, it is difficult to control the alignment and orientation of the CNTs in directly dispersing of CNTs to the resin; therefore, it has the difficulty to control the quality of the produced CNT-based composites.

Fracture toughness is one of the most important properties in many applications. Recently, some experimental studies have shown that using CNTs as the reinforcement can improve the fracture toughness [10–15]. The toughening mechanisms depend critically on the CNT/matrix interfacial behaviour which can be investigated through a CNT pullout test [16–19]. However, due to their extremely small size, only a few experimental studies have been carried out. Echeberria et al. [13] reported an increase in fracture toughness of multi-walled carbon nanotubes and single-walled carbon nanotubes reinforced alumina composites. They indicated that the pullout of CNTs and bridging are the reasons of the improved fracture toughness. Barber et al. [17] investigated the interfacial fracture energy using a single multi-walled CNT pullout test from a polymer matrix at a short embedded length. Their results suggested that a relatively strong interface with a high fracture energy. Lachman and Wagner [19] also found that the nanocomposite toughness increases with enhanced interfacial adhesion. They explained this result by using a pullout energy model and found that the pullout energy increases with the interfacial shear strength.

* Corresponding author. Tel.: +61 3 9902 0113; fax: +61 3 9905 1825.
E-mail address: wenyi.yan@monash.edu (W. Yan).

http://dx.doi.org/10.1016/j.compositesb.2015.07.003
1359-8368/© 2015 Elsevier Ltd. All rights reserved.

Besides the experimental work, many theoretical studies have been carried out to understand the mechanical performance of CNT reinforced composites [16,20–23]. Various approaches have been proposed by using molecular dynamic (MD) simulation [16,20,22,23]. For example, using molecular mechanics simulation, Liao and Li [16] investigated the interfacial characteristics of CNT reinforced polystyrene composite from pullout, including thermal residual radial stress, pullout energy and interfacial shear stress. Their result showed that the estimated interfacial shear stress ($\tau_s = 160$ MPa) is significantly higher than most carbon fibre reinforced polymer composite. Zheng et al. [20] used both molecular mechanics and MD simulations to estimate the interfacial shear strength, which is about 33 MPa. However the length of the CNT in the MD models was limited to the range of 4–10 nm due to the intensive computational requirements in the MD simulations [16,23–25].

The typical length of CNTs is in the order of a few microns, while the diameters range from less than 1 nm to about 30 nm that corresponds to an aspect ratio around 1000 [26]. The fracture toughness has the potential to be improved by increasing the CNT embedded length (interface length L_{CNT}) because of the increased interfacial area and therefore, increased energy dissipation. However, Chen et al. [27] carried out a theoretical study which showed that longer reinforcing CNTs do not definitely provide better fracture toughness on composites. For a strong adhesion between CNT and matrix, CNTs are fragmented with an increase in CNT length, which results in a sudden drop of the fracture toughness. In a weak adhesion between CNT and matrix interface, although the CNTs are pulled out, the improvement of fracture toughness quickly becomes saturated with an increase in CNT length.

To understand the bridging effect of CNT in the events of the fracture of CNT-reinforced composites, this paper investigates the single CNT pullout test by using cohesive zone modelling. The effect of interfacial bonding between CNT and epoxy matrix as well as CNT geometry effect on the debonding force are investigated, particularly on the effect of CNT embedded length. The bridging resistance of CNT is quantified by the specific pullout energy, pullout energy per unit interfacial area, in this research.

2. Finite element model for CNT pullout

Due to the limitations of computing time and resources of using MD method to study the pullout of CNTs, the finite element method is used to simulate the single CNT pullout at microscale in current study. In some other studies, CNTs have been described as a continuum solid beam or shell subjected to tension, bending, or torsional forces by applying continuum mechanics [25,26,28,29]. In this study, the continuum mechanics was applied to treat CNTs as membranes. Therefore, the nanoscale dimension of the wall thickness of the CNTs was excluded in the simulations. The nano- and the microscales problem becomes a single microscale problem.

In the single CNT pullout, a two-dimensional axisymmetric model at microscale was developed using a single cylindrical CNT embedded in a semi-infinite matrix. A pullout displacement was applied on the top of the CNT in the axial direction, as shown in Fig. 1(a). In this study, a 24 nm diameter carbon nanotube is embedded in an epoxy matrix with the embedded length $L_{CNT} = 2.6$ μm, which is consistent with the experiment by Cooper et al. [30]. The CNT and epoxy matrix were modelled as isotropic materials. The Young's modulus of CNT was taken as $E_{CNT} = 1.1$ TPa with the wall thickness = 0.34 nm, and epoxy matrix with $E_m = 3.4$ GPa was used in this study. The elastic Poisson's ratios of CNT ν_{CNT} and matrix ν_m, were kept respectively constant as 0.34 and 0.36 in all simulations. Membrane elements (MAX1) were used in commercial finite element package Abaqus to represent the cylindrical CNT as shown in Fig. 1(b). Membrane elements can be used to represent a thin surface in space which offers strength in the plane of the element without bending stiffness [31]. In addition, the axisymmetric cohesive elements (COHAX4) were used to define the cohesive zone between the interface of the CNT and the matrix.

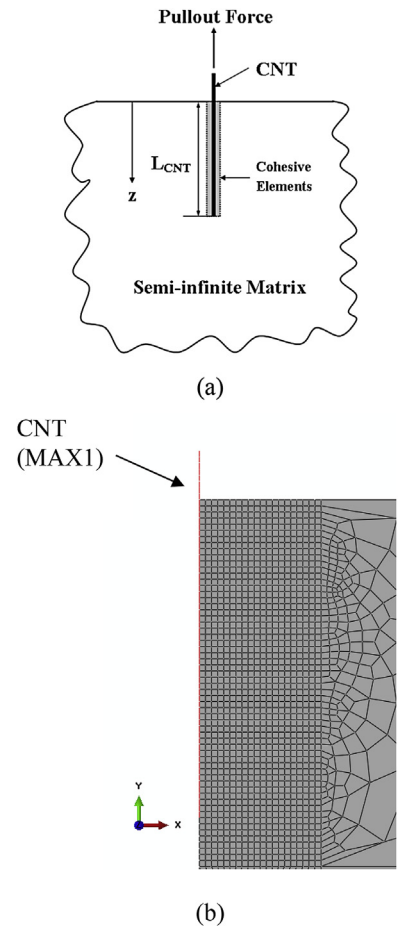

Fig. 1. (a) A schematic diagram of a single CNT pullout model; (b) Axisymmetric finite element model for a single CNT pullout: fine mesh around the interface.

Cohesive zone modelling is a commonly used technique to investigate the failure governed by crack or debonding propagation [32–34]. It uses the traction stress as a function of the separation at any point along a potential fracture path to describe the physical debonding/cracking process at that point. The area under the traction–separation curve is the fracture energy release rate, which is consistent with the concept in fracture mechanics to represent the energy required to create a unit fracture surface area. However, little attention has been paid to use cohesive zone modelling to simulate fibre pullout. Some researchers have derived the cohesive law for the CNT/polymer interface from the analysis of the weak van der Waals bonds [35–37]. The limitation of these analytical studies is that the cohesive laws derived are for an infinite length of CNT embedded in a polymer matrix. In addition, these proposed cohesive laws are too complicated to be applied in a finite element simulation. In this study, a cohesive zone model was adopted from Tvergaard [38] and Chaboche et al. [39]. As the previous study [40], a simplified cohesive zone model was used as

$$T_t = \left(\frac{27u_t^3}{4\delta_t^3} - \frac{27u_t^2}{2\delta_t^2} + \frac{27u_t}{4\delta_t}\right)\tau_{\max} \quad (1)$$

where u_t is the tangential separation, δ_t is the complete tangential separation, and τ_{max} is the interfacial crack initiation stress under shear loading condition. δ_d is the separation displacement of crack initiation, where crack surfaces start to separate at the peak shear stress as shown in Fig. 2. Correlating to energy-based fracture mechanics, the fracture energy release rate G_{IIc} is the area under the traction–separation curve.

3. CNT pullout results

3.1. Model validation

A comparison study between a finite element simulation at microscale and an experimental single CNT pullout test was carried out. Fig. 3 shows the simulated single CNT pullout curve. The numerical results were compared with the experimental results as shown in Table 1. W is the total CNT pullout energy, which is the total area under the pullout force–displacement curve. It can be seen that the numerical results are fitted overall very well with the experimental results listed by Cooper et al. [30] with these fitted parameters τ_{max} = 36 MPa, δ_d = 140 nm, and δ_t = 410 nm. In this case, the CNT pullout displacement corresponding to the maximum pullout force F_{max} is approximately 0.18 μm.

In addition, according to our previous work [44], the influence of frictional coefficient is negligible on the debonding force. This is because the friction only affects the pullout process after full debonding. Therefore, it is assumed that there is no friction during the pullout in this study.

3.2. Parametric study on CNT pullout

3.2.1. Interfacial bonding effect

The interfacial bonding effect is dependent on two dominant parameters, τ_{max} and δ_t, based on the cohesive law used in the single CNT pullout simulation (Eq. (1)). In this parametric study, τ_{max} varied from 15 MPa to 45 MPa and δ_t varied from 0.2 μm to 0.8 μm. A 24 nm diameter carbon nanotube with the embedded length L_{CNT} = 6.5 μm was used. The maximum pullout force F_{max}, the so called debonding force, is one of the most important parameters recorded from a pullout test, and it is used to calculate the average interfacial strength. Fig. 4 shows the relationship between the debonding force F_{max} and the interfacial crack initiation shear stress τ_{max} of the CNT/matrix interface. It clearly indicates that the debonding force increases almost linearly with the increase of the interfacial crack initiation shear stress in all the cases. The figure also indicates that the debonding force F_{max} slightly increases as the complete tangential separation δ_t increases.

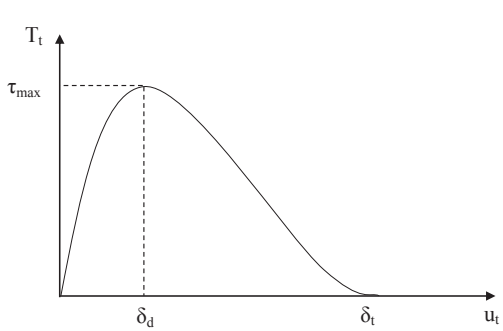

Fig. 2. Illustration of the cohesive law described by Eq. (1).

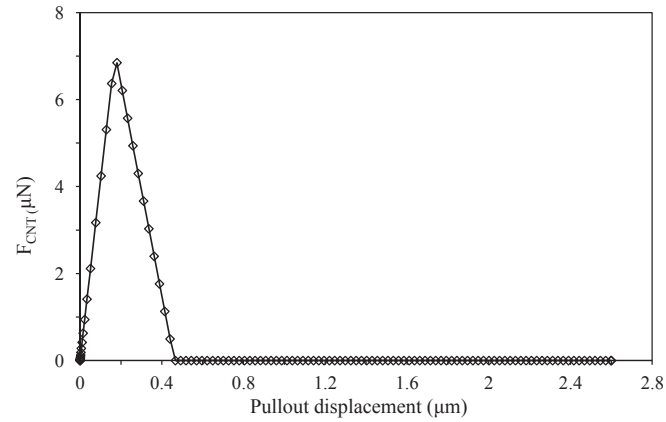

Fig. 3. Single CNT pullout curve from the microscale finite element simulation.

Table 1
Comparison between experiment and finite element simulation for single CNT pullout.

	FE simulation	Experiment [30]
Maximum pullout force F_{max} (μN)	6.845	6.8 ± 1.7
Total CNT pullout energy W (J)	1.63×10^{-12}	1.6×10^{-12}

3.2.2. CNT geometry effect

The effects of the CNT radius R_{CNT} and CNT embedded length L_{CNT} on the debonding force F_{max} are shown in Fig. 5. The CNT radius was selected from 0.005 to 0.05 μm [41] and CNT embedded length ranged from 0.5 to 50 μm. Both figures show that the debonding force increases with CNT radius R_{CNT}. In Fig. 5(b), the interesting finding is that the increase of debonding force becomes saturated when the CNT embedded length L_{CNT} is over 20 μm, which means that increasing CNT embedded length is not definitely able to continuously increase the debonding force on CNT pullout. Therefore, it can be inferred that the debonding force will reach to a saturated value at a critical embedded length. This critical CNT embedded length will be identified from further discussion in Section 4.

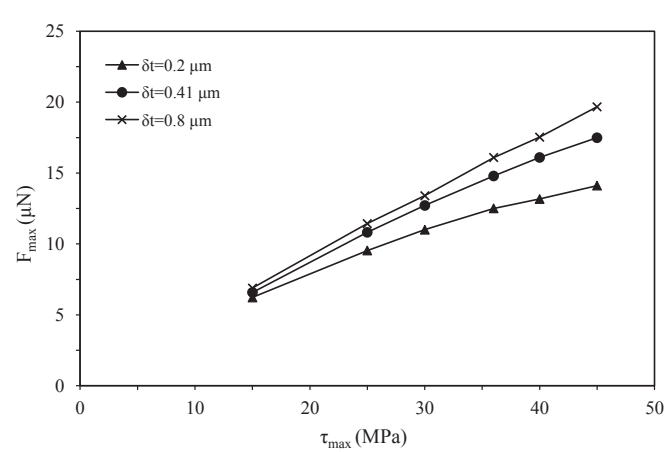

Fig. 4. Influence of interfacial crack initiation shear stress τ_{max} on the debonding force with different values of complete separation displacement δ_t.

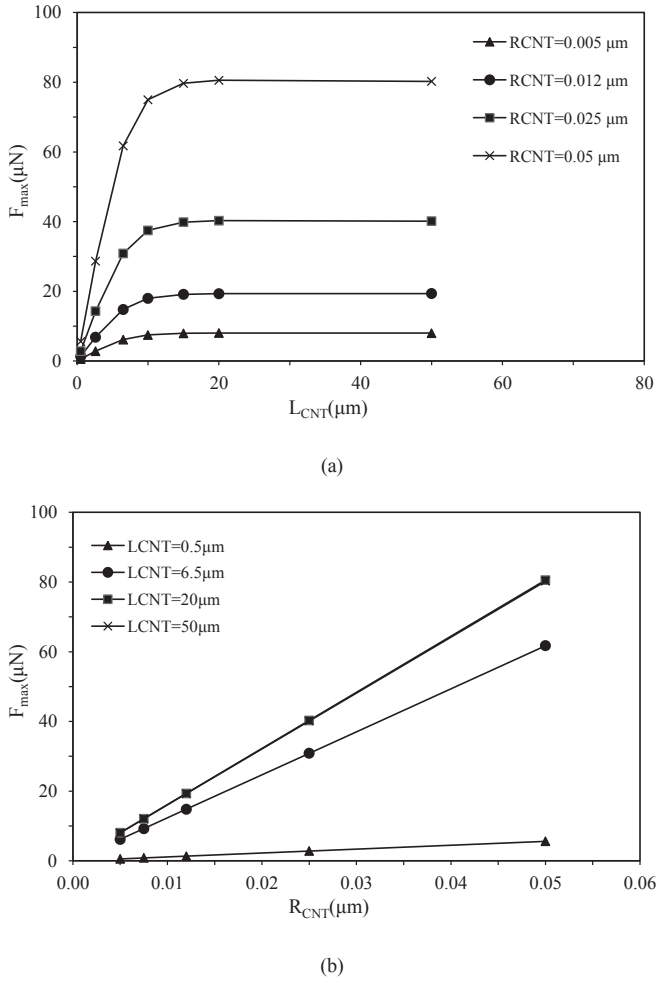

Fig. 5. Influence of (a) CNT embedded length L_{CNT} and (b) CNT radius R_{CNT} on the debonding force.

In addition, the effect of CNT embedded length on interfacial shear strength τ_s was examined. The interfacial shear strength is defined as [42].

$$\tau_s = \frac{F_{\max}}{2\pi R_{CNT} L_{CNT}} \tag{2}$$

The effect of the CNT embedded length L_{CNT} on the interfacial shear strength τ_s is shown in Fig. 6. It can be seen that the interfacial shear strength is not a constant, which decreases as the increases of the CNT embedded length. It means that longer CNTs do not definitely result in better fracture toughness of CNT-reinforced composites. The similar trend was also observed in the study by Meguid et al. [43] at atomic scale. Additionally, Fig. 6 shows that the radius of the CNT has no significant effect on the interfacial shear strength. Similar conclusion was obtained in traditional carbon fibre composites [44]. In fact, according to the definition of Eq. (2), the interfacial shear strength doesn't represent the intrinsic interfacial fracture toughness. The effect of CNT embedded length on the interfacial shear strength cannot be theoretically excluded. It is recommended to use this concept with caution in practice.

3.3. Bridging effect of CNT in CNT pullout

CNT bridging plays an important role in toughening CNT reinforced composites. The toughening effect is largely dictated by the

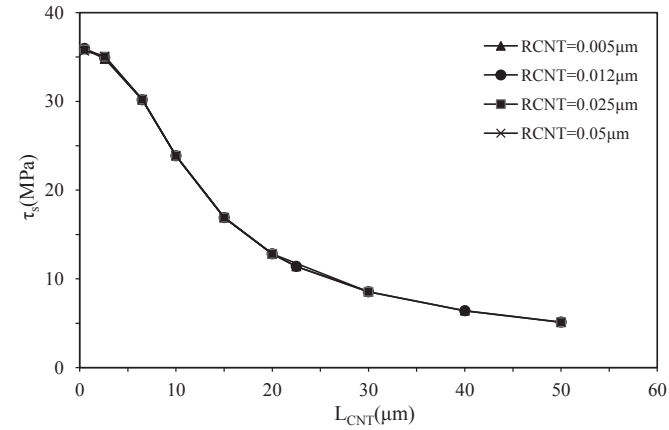

Fig. 6. Influence of CNT embedded length L_{CNT} and CNT radius R_{CNT} on the interfacial shear strength.

conditions of the interface between the reinforcing CNT and polymer matrix. Fibre bridging is the case where the strength of the interface exceeds the reinforcing CNT and the CNT exerts a force across the width of a crack to prevent the crack from further developing. Fibre bridging appears behind a major crack tip in an intralaminar fracture, which enhances the fracture resistance of fibre reinforced composite.

In this study, specific pullout energy, an energy-based approach, is used to evaluate the bridging effect of CNTs during the pullout. The specific pullout energy of CNT ω_{CNT}, pullout energy per unit interfacial area, is defined as

$$\omega_{CNT} = \frac{W_{CNT}}{2\pi R_{CNT} L_{CNT}} \tag{3}$$

where W_{CNT} is the total CNT pullout energy, which is the total area under the pullout force–displacement curve. The method used in this study is based on the displacement-controlled test which is commonly used for macroscale fracture specimens [45] and the kinetic energy is neglected.

According to Fig. 7, the specific pullout energy increases with the increased CNT embedded length. The figure also shows that the specific pullout energy is independent of the CNT radius, which means increasing CNT embedded length without changing the CNT radius may enhance the fibre bridging effect. Lu and Bhattachary

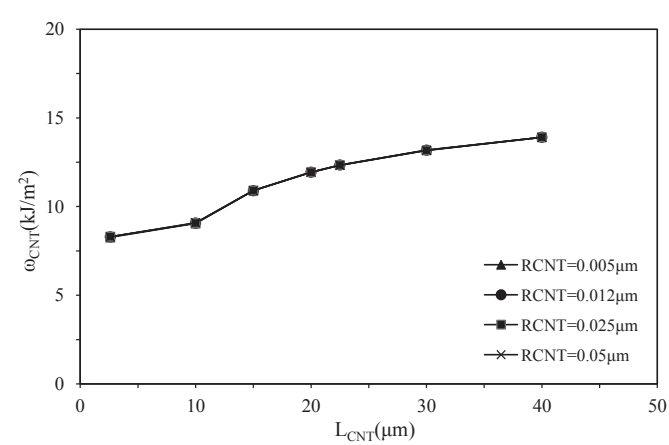

Fig. 7. Influence of CNT embedded length L_{CNT} and CNT radius R_{CNT} on the specific pullout energy.

[45] also showed that the longer nanotubes have a higher fracture resistance than the shorter tubes and the fracture energy is not much dependent on the diameter of the CNTs. In the experimental study of Mirjalili and Hubert [12], it was also concluded that the fracture toughness can be improved by increasing the length of CNTs.

4. Saturated debonding force and critical CNT embedded length

4.1. Identification of saturated debonding force F_{sat} and critical CNT embedded length $L_{c(CNT)}$

As shown in Fig. 5(a), the debonding force approaches a saturated value when the embedded length of CNT reaches a critical value. In order to accurately identify the critical embedded length $L_{c(CNT)}$ corresponding to the saturated debonding force F_{sat}, more numerical simulations with different CNT embedded lengths were carried out. In this study, a fixed radius ($R_{CNT} = 0.012$ μm) with these fitted cohesive parameters $\tau_{max} = 36$ MPa, $\delta_d = 140$ nm, and $\delta_t = 410$ nm were used. As shown in Fig. 8, the debonding force becomes saturated ($F_{sat} \approx 19.35$ μN) as the CNT embedded length at 22.5 μm. In this case, the $L_{CNT} = 22.5$ μm is considered as the critical CNT embedded length, i.e., $L_{c(CNT)} = 22.5$ μm. When $L_{CNT} < L_{c(CNT)}$, the debonding force increases with CNT embedded length L_{CNT}. When$L_{CNT} \approx L_{c(CNT)}$ or $L_{CNT} > L_{c(CNT)}$, the debonding force asymptotically becomes saturated. This numerical result indicates that the debonding force cannot be continuously increased by increasing the CNT embedded length, and the increasing is only effective for short CNTs.

To verify this interesting finding, the distribution of shear stresses along the interface between the CNT and the matrix are shown in Fig. 9. Four cases were selected from Fig. 8 as the examples to show the distribution of the shear stress along the interface for $L_{CNT} = 6.5$ μm, 17.5 μm, 22.5 μm, and 32.5 μm. The debonding force F_{max} was calculated according to the relation of

$$F = 2\pi R_{CNT} \int_0^{L_{CNT}} \tau dL. \tag{4}$$

Fig. 9(a–c) show that the area under stress distribution increases as the increase of CNT embedded length, which results in the increase of the debonding force. Beyond point 3, the distribution of the shear stress along the interface will not change. It only shifts with the debonding crack growth. Therefore, the area under stress distribution does not increase further (Fig. 9(d)) and hence a constant saturated debonding force exists. These results confirm that the debonding force increases initially as the increase of CNT embedded lengths and it becomes saturated as the CNT embedded length exceeds the critical embedded length.

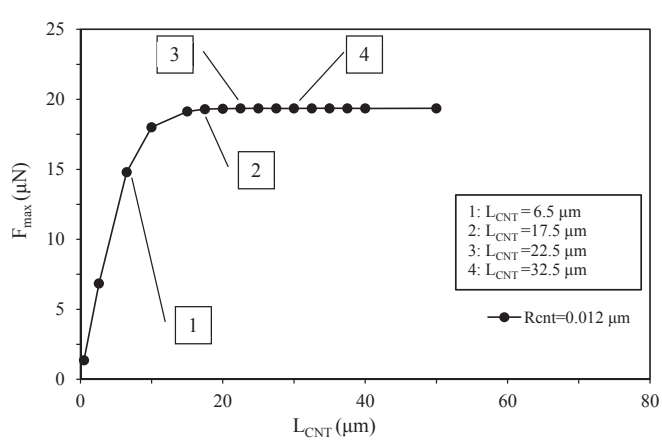

Fig. 8. Identification of saturated debonding force F_{sat} corresponding to the CNT critical length $L_{c(CNT)}$.

Practically, CNT will break if the maximum axial tensile stress in CNT during pullout reaches its tensile strength. The tensile strength of CNT was reported to be up to 150 GPa [9]. To break a CNT with the strength of 150 GPa, the critical axial force is estimated as 67.8 μN, which is higher than the saturated debonding force of 19.35 μN obtained in this study. It indicates that the CNT will not break in this pullout case. For the CNT with the given cross-section to break due to tensile failure before reaching the saturated debonding force of 19.35 μN, its tensile strength should be less than 42.8 GPa. Due to the scatter of reported data of CNT tensile strength in literature [46–48], the influence of CNT break is not discussed in following parametrical study. Practically, it should be considered in estimating the maximum pullout force and CNT embedded length once the CNT tensile strength is known.

4.2. Parametrical study on saturated debonding force and critical CNT embedded length

As shown in Fig. 5, the debonding force approaches a saturated value F_{sat} when CNT embedded length reach to a critical value. In general, the saturated debonding force is a function of the parameters,

$$F_{sat} = f(\tau_{\max}, \delta_t, R_{CNT}, E_{CNT}, E_m, \nu_{CNT}, \nu_m) \tag{5}$$

and the critical CNT embedded length ($L_{c(CNT)}$) is a function of the parameters,

$$L_{c(CNT)} = f(\tau_{\max}, \delta_t, R_{CNT}, E_{CNT}, E_m, \nu_{CNT}, \nu_m) \tag{6}$$

The parameters, ν_{CNT} and ν_m (elastic Poisson's ratio) are dimensionless. Finite element simulations were carried out to numerically investigate the functional dependency of the listed parameters in Eqs. (5) and (6) on the saturated debonding force and critical CNT embedded length, respectively. The elastic Poisson's ratios, ν_{CNT} and ν_m, are kept respectively constant as 0.34 and 0.36. Young's modulus of CNT $E_{CNT} = 1.1$ TPa and Young's modulus of matrix $E_m = 3.4$ GPa are used in all of following simulations. Both of the saturated debonding force F_{sat} and critical length, $L_{c(CNT)}$, were examined as each parameter, except ν_{CNT} and ν_m, varied individually in the simulation, whilst all other parameters were kept constant at their nominal values as shown in Table 2.

4.2.1. Interfacial bonding effect

The interfacial bonding effect is dependent on two dominant parameters, τ_{max} and δ_t, based on the cohesive law used in the single CNT pullout simulation (Eq. (1)). As the result obtained in Section 4.1, the debonding force approaches a saturated value F_{sat} when CNT embedded length reaches to a critical value, which is $L_{c(CNT)} = 22.5$ μm in this case. Therefore a single CNT with embedded length $L_{CNT} = 35$ μm, which is larger than the critical value, was used in this simulation to investigate the interfacial bonding effect on the saturated debonding force.

Fig. 10 shows the relationship between the saturated debonding force F_{sat} and the interfacial crack initiation shear stress τ_{max}. It clearly indicates that the debonding force increases almost linearly with the interfacial crack initiation shear stress in all the cases. The saturated debonding force also increases as the increase of complete tangential separation. These numerical results indicate that if the interface has a stronger bonding between the CNT and the matrix, a higher saturated debonding force can be identified.

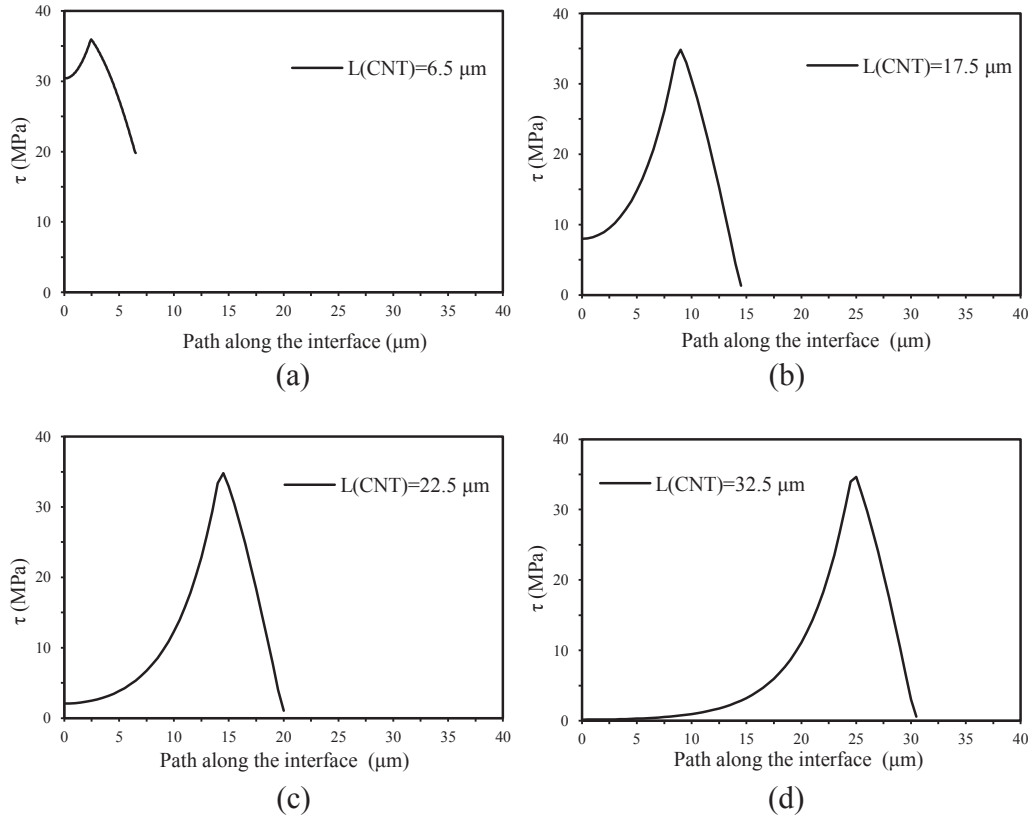

Fig. 9. Shear stresses distribution along CNT/matrix interface for 4 different CNT embedded lengths, corresponding to the 4 cases in Fig. 8.

Table 2
Nominal, minimum and maximum values for investigated parameters.

Parameter	Nominal	Min	Max
Interfacial crack initiation shear stress (MPa) τ_{max}	36	15	45
Complete tangential separation (μm) δ_t	0.41	0.2	0.8
CNT radius (μm) R_{CNT}	0.012	0.005	0.05

Fig. 11 shows the relationship between the critical CNT embedded length ($L_{c(CNT)}$) and the interfacial crack initiation shear stress (τ_{max}) for different complete tangential separation δ_t. It clearly shows that the critical CNT embedded length decreases almost linearly as the increase of the interfacial crack initiation shear stress, and also decreases with the increase of the complete tangential separation. The numerical results indicate that if the interface contains strong chemical bonding, the debonding force can approach the saturated value more rapidly.

4.2.2. Effect of CNT radius and material properties

The effect of the CNT radius R_{CNT} on the saturated debonding force F_{sat} is shown in Fig. 12. It can be seen that the saturated debonding force increases with the increase in the CNT radius R_{CNT}. This is due to that the CNT pullout force F_{max} increases linearly with the CNT radius R_{CNT}. This numerical result indicates that increasing the radius of CNT, a higher saturated debonding force can be achieved.

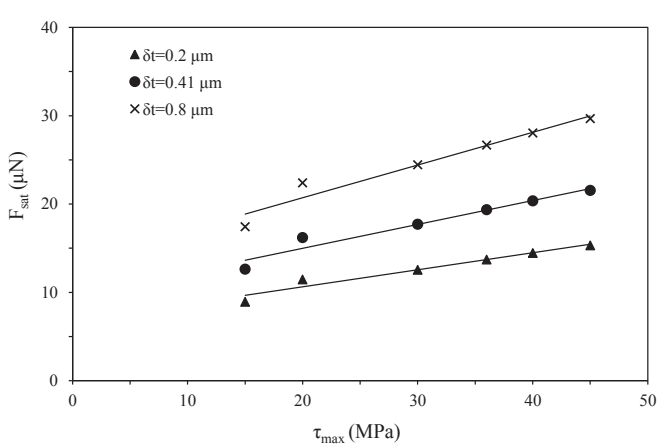

Fig. 10. Influence of interfacial crack initiation shear stress τ_{max} on saturated debonding force for different complete separation displacement δ_t.

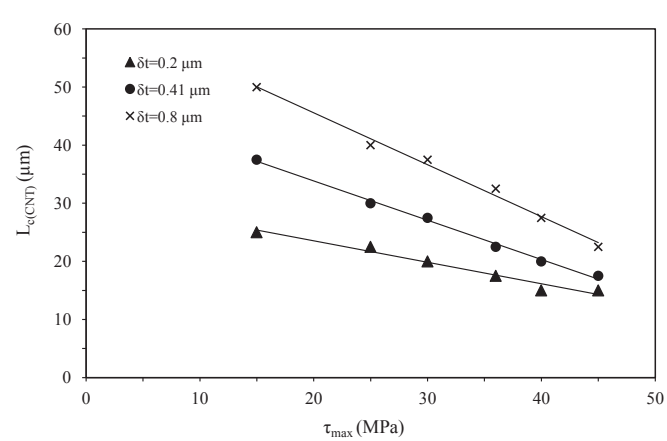

Fig. 11. Influence of interfacial crack initiation shear stress on the critical CNT embedded length for different complete separation displacement δ_t.

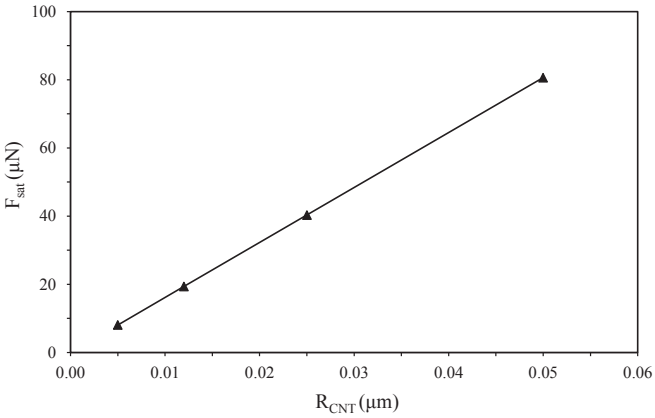

Fig. 12. Influence of CNT radius R_{CNT} on the saturated debonding force.

The effect of the CNT radius R_{CNT} on the critical CNT embedded length $L_{c(CNT)}$ is shown in Fig. 13. It can be seen that the radius of the CNT has no significant effect on the critical embedded length. It means that changing the radius of CNT does not influence the identification of critical CNT embedded length.

5. Conclusions

The finite element method was applied to simulate the single CNT pullout with the assistance of the cohesive zone model. The main conclusions of this research are summarised below.

(1) The numerical results clearly indicate that the debonding force increases almost linearly with the increase of interfacial crack initiation shear stress in all the cases, and also slightly increases with the complete tangential separation.
(2) Specific pullout energy, pullout energy per unit interfacial area, is used in this paper as a measure of the fracture resistance, which can be well used to quantify the bridging effect of the CNTs during the pullout. The numerical results indicate that the specific pullout energy increases with the increased CNT embedded length, while it is independent of the CNT radius. Therefore, increasing CNT embedded length without changing the CNT radius may enhance the fibre bridging effect.
(3) A saturated debonding force exists corresponding to a critical CNT embedded length. This is verified by the distribution of the shear stress along the interface between the CNT and the matrix. As the area under stress distribution does not increase further once the CNT embedded length exceeds the critical length, a saturated constant debonding force exists. This numerical result indicates that the debonding force cannot be continuously increased by increasing the CNT embedded length, and the increasing is only effective for short CNTs.
(4) The parametric study shows that a higher saturated debonding force can be achieved if the CNT has a larger radius or the interface between the CNT and the matrix has a stronger bonding. The critical CNT embedded length decreases with the increase of the interfacial crack initiation shear stress, while it is independent of the CNT radius.

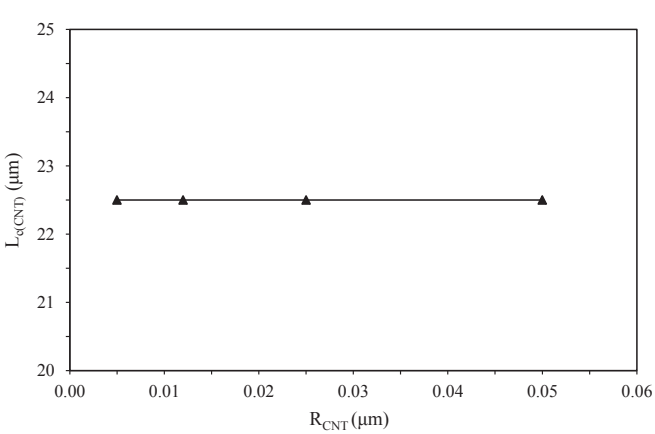

Fig. 13. Influence of CNT radius R_{CNT} on the critical CNT embedded length.

The findings such as those on saturated debonding force and critical CNT embedded length can be used as guidelines in the development of CNT or other fibre reinforced composites.

References

[1] Ajayan PM, Schadler LS, Braun PV. Nanocomposite science and technology. Weinheim: Wiley; 2003.
[2] Zhu Y, Murali S, Cai W, Li X, Suk JW, Potts JR, et al. Graphene and graphene oxide: synthesis, properties, and applications. Adv Mater 2010;22(35):3906–24.
[3] Qian D, Dickey EC, Andrews R, Rantell T. Load transfer and deformation mechanisms in carbon nanotube-polystyrene composites. Appl Phys Lett 2000;76(20):2868–70.
[4] Chang TE, Jensen LR, Kisliuk A, Pipes RB, Pyrz RB, Sokolov AP. Microscopic mechanism of reinforcement in single-wall carbon nanotube/polypropylene nanocomposite. Polymer 2005;46(2):439–44.
[5] Beckman W. UC researchers Shatter World Records with length of carbon nanotube arrays. 2007 [cited 06–11/2012]; Available from: http://www.uc.edu/News/NR.aspx?ID=5700.
[6] Iijima S. Helical microtubules of graphite carbon. Nature 1991;354:56–8.
[7] Wong EW, Sheehan PE, Lieber CM. Nanobeam mechanics: elasticity, strength and toughness of nanorods and nanotubes. Science 1997;277(5334):1971–5.
[8] Treacy MMJ, Ebbesen TW, Gibson JM. Exceptionally high Young's modulus observed for individual carbon nanotubes. Nature 1996;381(6584):678.
[9] Demczyk BG, Wang YM, Cumings J, Hetman M, Han W, Zettl A, et al. Direct mechanical measurement of the tensile strength and elastic modulus of multiwalled carbon nanotubes. Mater Sci Eng A 2002;334(1–2):173–8.
[10] Schulte K, Gojny FH, Wichmann MHG, Fiedler B. Influence of different carbon nanotubes on the mechanical properties of epoxy matrix composites – a comparative study. Compos Sci Technol 2005;65(15–16):2300–13.
[11] Seyhan AT, Tanoglu M, Schulte K. Tensile mechanical behavior and fracture toughness of MWCNT and DWCNT modified vinyl-ester/polyester hybrid nanocomposites produced by 3-roll milling. Mater Sci Eng A 2009;523(1–2):85–92.
[12] Mirjalili V, Hubert P. Modelling of the carbon nanotube bridging effect on the toughening of polymers and experimental verification. Compos Sci Technol 2010;70(10):1537–43.
[13] Echeberria J, Rodriguez N, Vleugels J, Vanmeensel K, Reyes-Rojas A, Garcia-Reyes A, et al. Hard and tough carbon nanotube-reinforced zirconia-toughened alumina composites prepared by spark plasma sintering. Carbon 2012;50(2):706–17.
[14] Almuhammadi K, Alfano M, Yang Y, Lubineau G. Analysis of interlaminar fracture toughness and damage mechanisms in composite laminates reinforced with sprayed multi-walled carbon nanotubes. Mater Des 2014;53(0):921–7.
[15] Lau KT, Lu M, Hui D. Coiled carbon nanotubes: synthesis and their potential applications in advanced composite structures. Compos Part B Eng 2006;37(6):437–48.
[16] Liao K, Li S. Interfacial characteristics of a carbon nanotube-polystyrene composite system. Appl Phys Lett 2001;79(25):4225–7.
[17] Barber AH, Cohen SR, Kenig S, Wagner HD. Interfacial fracture energy measurements for multi-walled carbon nanotubes pulled from a polymer matrix. Compos Sci Technol 2004;64(15 SPEC. ISS.):2283–9.
[18] Gojny FH, Nastalczyk J, Roslaniec Z, Schulte K. Surface modified multi-walled carbon nanotubes in CNT/epoxy-composites. Chem Phys Lett 2003;370(5–6):820–4.
[19] Lachman N, Wagner HD. Correlation between interfacial molecular structure and mechanics in CNT/epoxy nano-composites. Compos Part A Appl Sci Manuf 2010;41(9):1093–8.
[20] Zheng Q, Xia D, Xue Q, Yan K, Gao X, Li Q. Computational analysis of effect of modification on the interfacial characteristics of a carbon nanotube-polyethylene composite system. Appl Surf Sci 2009;255(6):3534–43.
[21] Tan X, Kin L. A nonlinear pullout model for unidirectional carbon nanotube-reinforced composites. Compos Part B Eng 2004;35B(3):211–7.

[22] Pregler SK, Byeong-Woo J, Sinnott SB. Ar beam modification of nanotube based composites using molecular dynamics simulations. Compos Sci Technol 2008;68(9):2049–55.
[23] Liu YJ, Nishimura N, Qian D, Adachi N, Otani Y, Mokashi V. A boundary element method for the analysis of CNT/polymer composites with a cohesive interface model based on molecular dynamics. Eng Anal Bound Elem 2008;32(4):299–308.
[24] Kulkarni M, Carnahan D, Kulkarni K, Qian D, Abot JL. Elastic response of a carbon nanotube fiber reinforced polymeric composite: a numerical and experimental study. Compos Part B Eng 2010;41(5):414–21.
[25] Fan CW, Liu YY, Hwu C. Finite element simulation for estimating the mechanical properties of multi-walled carbon nanotubes. Appl Phys A Mater Sci Process 2009;95(3):819–31.
[26] Namilae S, Chandra N. Multiscale model to study the effect of interfaces in carbon nanotube-based composites. J Eng Mater Technol Trans ASME 2005;127(2):222–32.
[27] Chen YL, Liu B, He XQ, Huang Y, Hwang KC. Failure analysis and the optimal toughness design of carbon nanotube-reinforced composites. Compos Sci Technol 2010;70(9):1360–7.
[28] Fan C-W, Huang J-H, Hwu C, Liu Y-Y. Mechanical properties of single-walled carbon nanotubes – a finite element approach. Adv Mater Res 2008;33–37(2):937–42.
[29] Huang J, Rodrigue D. Equivalent continuum models of carbon nanotube reinforced polypropylene composites. Mater Des 2013;50(0):936–45.
[30] Cooper CA, Cohen SR, Barber AH, Wagner HD. Detachment of nanotubes from a polymer matrix. Appl Phys Lett 2002;81(20):3873–5.
[31] ABAQUS 6.11 Documentation: Dassault Systèmes Simulia Corp. 2012.
[32] Taljsten B. Strengthening of concrete prism using the plate-bonding technique. Int J Fract 1996;82(3):253–66.
[33] Teng JG, Yuan H, Chen JF. FRP-to-concrete interfaces between two adjacent cracks: theoretical model for debonding failure. Int J Solids Struct 2006;43(18–19):5750–78.
[34] Tsai JH, Patra A, Wetherhold R. Finite element simulation of shaped ductile fiber pullout using a mixed cohesive zone/friction interface model. Compos Part A Appl Sci Manuf 2005;36(6):827–38.
[35] Jiang LY. A cohesive law for carbon nanotube/polymer interface accounting for chemical covalent bonds. Math Mech Solids 2010;15(7):718–32.
[36] Jiang LY, Huang Y, Jiang H, Ravichandran G, Gao H, Hwang KC, et al. A cohesive law for carbon nanotube/polymer interfaces based on the van der Waals force. J Mech Phys Solids 2006;54(11):2436–52.
[37] Tan H, Jiang LY, Huang Y, Liu B, Hwang KC. The effect of van der Waals-based interface cohesive law on carbon nanotube-reinforced composite materials. Compos Sci Technol 2007;67(14):2941–6.
[38] Tvergaard V. Effect of fibre debonding in a whisker-reinforced metal. Mater Sci Eng A 1990;A125(2):203–13.
[39] Chaboche JL, Girard R, Levasseur P. On the interface debonding models. Int J Damage Mech 1997;6(3):220–57.
[40] Jia Y, Chen Z, Yan W. A numerical study on carbon nanotube-hybridized carbon fibre pullout. Compos Sci Technol 2014;91:38–44.
[41] Baughman RH, Zakhidov AA, De Heer WA. Carbon nanotubes – the route toward applications. Science 2002;297(5582):787–92.
[42] Daniel IM, Ishai O. Engineering mechanics of composite materials. 2nd ed. New York: Oxford University Press; 2006.
[43] Meguid SA, Wernik JM, Al Jahwari F. Toughening mechanisms in multiphase nanocomposites. Int J Mech Mater Des 2013;9(2):115–25.
[44] Jia Y, Yan W, Liu H-Y. Carbon fibre pullout under the influence of residual thermal stresses in polymer matrix composites. Comput Mater Sci 2012;62:79–86.
[45] Lu Q, Bhattacharya B. Fracture resistance of zigzag single walled carbon nanotubes. Nanotechnology 2006;17(5):1323–32.
[46] Yu MF, Lourie O, Dyer MJ, Moloni K, Kelly TF, Ruoff RS. Strength and breaking mechanism of multiwalled carbon nanotubes under tensile load. Science 2000;287(5453):637–40.
[47] Tran CD, Humphries W, Smith SM, Huynh C, Lucas S. Improving the tensile strength of carbon nanotube spun yarns using a modified spinning process. Carbon 2009;47(11):2662–70.
[48] Xiao T, Ren Y, Liao K, Wu P, Li F, Cheng HM. Determination of tensile strength distribution of nanotubes from testing of nanotube bundles. Compos Sci Technol 2008;68(14):2937–42.